

# Unprocessing Seven Years of Algorithmic Fairness

André F. Cruz

Moritz Hardt

*Max Planck Institute for Intelligent Systems, Tübingen and Tübingen AI Center*

## Abstract

Seven years ago, researchers proposed a postprocessing method to equalize the error rates of a model across different demographic groups. The work launched hundreds of papers purporting to improve over the postprocessing baseline. We empirically evaluate these claims through thousands of model evaluations on several tabular datasets. We find that the fairness-accuracy Pareto frontier achieved by postprocessing contains all other methods we were feasibly able to evaluate. In doing so, we address two common methodological errors that have confounded previous observations. One relates to the comparison of methods with different unconstrained base models. The other concerns methods achieving different levels of constraint relaxation. At the heart of our study is a simple idea we call unprocessing that roughly corresponds to the inverse of postprocessing. Unprocessing allows for a direct comparison of methods using different underlying models and levels of relaxation. Interpreting our findings, we recall a widely overlooked theoretical argument, present seven years ago, that accurately predicted what we observe.

## 1 Introduction

Risk minimizing predictors generally have different error rates in different groups of a population. When errors are costly, some groups therefore seem to bear the brunt of uncertainty, while others enjoy the benefits of optimal prediction. This fact has been the basis of intense debate in the field of algorithmic fairness, dating back to the 1950s [17]. A difference in error rates between groups, equally deserving of a resource, strikes many as a moral wrong [2, 4].

Researchers have therefore proposed numerous algorithmic interventions to mitigate a disparity in error rates. The most basic such method is known as postprocessing. Postprocessing sets group-specific acceptance thresholds so as to minimize risk while achieving an equality in error rates across a desired set of groups. Postprocessing is both simple and computationally efficient.

Perhaps because of its simplicity, postprocessing has been widely assumed to be sub-optimal. Troves of academic contributions seek to improve over postprocessing by more sophisticated algorithmic means. These efforts generally fall into two categories. Preprocessing methods aim to adjust the source data in such a manner that predictors trained on the data satisfy certain properties. So-called “inprocessing” methods, in contrast, modify the training algorithms itself to achieve a desired constraint during the optimization step.

### 1.1 Our contributions

Through a large, computationally intensive meta study we empirically establish that postprocessing is Pareto-dominant among all methods we were feasibly able to evaluate. Whatever level of accuracy can be achieved by any method at a specific level of error rate disparity, can also be achieved by setting group-specific acceptance thresholds on an unconstrained risk score.

We performed more than ten thousand model training and evaluation runs across five different prediction tasks from the `folktables` package [13], based on tabular data from the US Census

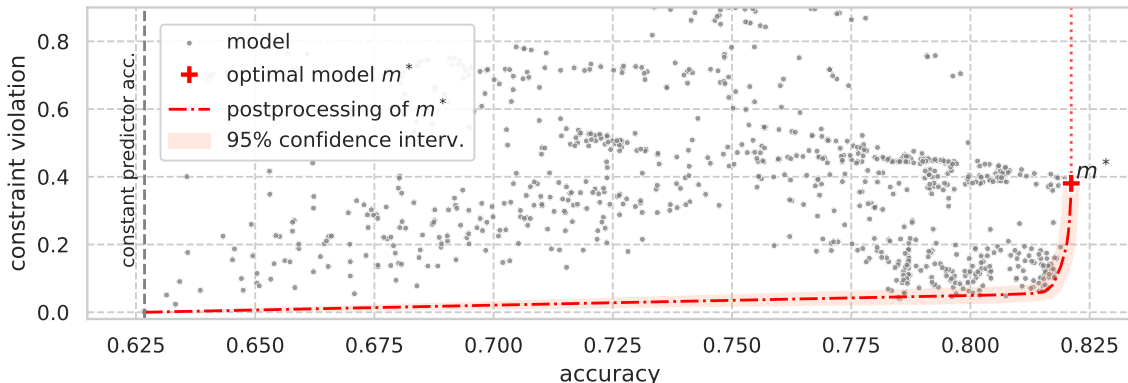


Figure 1: Fairness and constraint violation for 1000 models trained on the ACSIncome dataset [13], corresponding to a variety of preprocessing or inprocessing methods, as well as standard unconstrained learners. Shown in red is the postprocessing Pareto frontier of the *single* model with highest accuracy.

American Community Survey. The methods include recent state-of-the-art algorithms, as well as standard baselines. While postprocessing is hyperparameter-free, we did extensive search for the best hyperparameters of all competing methods.

Our work addresses two common methodological errors that have confounded previous comparisons with postprocessing.

First, many preprocessing and inprocessing methods naturally do not achieve exact error rate equality, but rather some relaxation of the constraint. In contrast, postprocessing is typically applied so as to achieve exact equality. The primary reason for this seems to be that there is a simple and efficient method based on tri-search to achieve exact equality [16]. However, an efficient relaxation of error rate parity is more subtle and is therefore lacking from popular software packages. We contribute a linear programming formulation to achieve approximate error rate parity for postprocessing.<sup>1</sup> This allows us to compare methods to postprocessing at the same level of slack.

Second, different methods use base models of varying performance. Observed improvements may therefore be due to a better unconstrained base model rather than a better way of achieving error rate parity. How can we put different methods on a level playing field? We introduce a simple idea we call *unprocessing* that roughly corresponds to the inverse of postprocessing. Here, we take a model that satisfies error rate parity (approximately) and optimize group-specific thresholds so as to yield the best *unconstrained* model possible. Unprocessing maps any fairness-constrained model to a corresponding unconstrained counterpart, to which we can then apply postprocessing. When comparing postprocessing to any given method we therefore do not have to come up with our own unconstrained model. We can simply steal, so to say, the unconstrained model implicit in the method.

These findings should not come as a surprise. Theory, perhaps overlooked, had long contributed an important fact: If an unconstrained predictor is close to Bayes optimal (in squared loss), then postprocessing this predictor is close to optimal among all predictors satisfying error rate parity [16, Theorem 4.5]. To be sure, this theorem applies to the squared loss and there are clever counterexamples in some other cases [25]. However, our empirical evaluation suggests that these counterexamples don’t arise in the real datasets we considered. This may be the case because, on the tabular datasets we consider, methods such as gradient boosting produce scores that are likely close to Bayes optimal under the squared loss.

<sup>1</sup>Open-source python package: <https://github.com/AndreFCruz/error-parity>

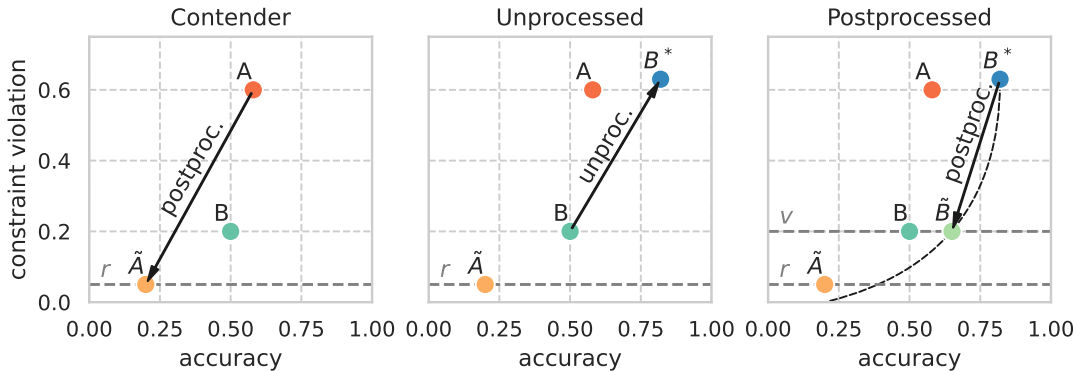


Figure 2: Example illustrating unprocessing. Left: Initial unconstrained model  $A$  postprocessed to  $\tilde{A}$ . Some contender model  $B$  incomparable to  $\tilde{A}$ . Middle: We unprocess  $B$  to get a new model  $B^*$ . Right: Postprocessing  $B^*$  to the same constraint level as  $B$ .

**Limitations and broader impacts.** We are narrowly concerned with evaluating algorithms that achieve error rate parity approximately. We do not contribute any new substantive insights about fairness in different domains. Nor do we escape the many valid criticisms that have been brought forward against algorithmic fairness narrowly construed [3, 4, 18]. In particular, our work says nothing new about the question whether we should equalize error rates in the first place. Some argue that error rates should be a diagnostic, not a locus of intervention [4]. Others reject the idea altogether [8]. If, however, the goal is to equalize error rates exactly or approximately, the simplest way of doing so is optimal: *Take the best available unconstrained model and optimize over group-specific thresholds.*

## 1.2 Related work

Hardt, Price, and Srebro [16] introduced error rate parity under the name of *equalized odds* in the context of machine learning and gave an analysis of postprocessing, including the aforementioned tri-search algorithm and theoretical fact. Woodworth et al. [25] proposed a relaxation of equalized odds and an algorithm to achieve the relaxation, as well as examples of specific loss functions and predictors for which postprocessing is not optimal.

Numerous works have considered constrained empirical risk formulations to achieve fairness criteria, see, e.g., [1, 7, 9, 10, 14, 21, 26] for a starting point. The work on learning fair representations [27] spawned much follow-up work on various preprocessing methods. See Section 2 for an extended discussion of the related work that we draw on in our experiments. We are unable to survey the vast space of algorithmic fairness methods here.

The basis of our evaluation are the prediction tasks made available by the `folktables` package [13].

## 2 Experimental setup

We conduct experiments on four standard machine learning models, paired with five popular algorithmic fairness methods. The standard unconstrained models in the comparison are: gradient boosting machine (GBM), random forest (RF), neural network (NN), and logistic regression (LR).

Regarding fairness interventions, we include both pre- and inprocessing methods in our experiments. We use the learned fair representations (LFR) [27] and the correlation remover (CR) [5] preprocessing fairness methods, respectively implemented in the `aif360` and `fairlearn` Python

libraries. Additionally, we use the exponentiated gradient reduction (EG) and the grid search reduction (GS) inprocessing fairness methods [1] (implemented in `fairlearn`), as well as the FairGBM [10] inprocessing method (implemented in `fairgbm`). The preprocessing methods (CR, LFR) can be paired with any other ML model ( $2 \cdot 4 = 8$  pairs), EG as well (4 pairs), and GS is compatible with GBM, RF, and LR models (3 pairs). FairGBM is naturally only compatible with GBM. Together with the four standard unconstrained models, there is a total of 20 different methods (or pairings) in the comparison.

Although there have been numerous proposed fairness methods over the years, far fewer have available and ready-to-use open-source implementations. This is somewhat inevitable, as every new method is compatible with a restricted set of fairness criteria or, in the case of ensemble methods (e.g., EG, GS) a restricted set of base learners. Postprocessing approaches have a practical advantage: a single implementation is compatible with any underlying learner that can produce scores of predicted probabilities, and any fairness criterion that can be expressed as a constraint over the joint distribution of  $(Y, \hat{Y}, S)$ , where  $Y$  is the true target,  $\hat{Y}$  the predictions, and  $S$  the protected group membership.

On each dataset, we train 50 instances of each ML algorithm in the study. For clarity, we will refer to different pairs of  $\langle \text{unconstrained, fairness-aware} \rangle$  algorithms as different algorithms (e.g.,  $\langle \text{GBM, EG} \rangle$  and  $\langle \text{NN, EG} \rangle$  are two different algorithms). As we study 20 different ML algorithms, a total of  $50 \cdot 20 = 1000$  ML models is trained on each dataset. Each model is trained with a different randomly-sampled selection of hyperparameters (e.g., learning rate of a GBM, number of trees of an RF, weight regularization of an LR). This fulfills two goals: first, to accurately explore the best outcomes of competing fair ML methods, as related work has shown that a wide range of fairness values can be obtained for the same ML algorithm by simply varying its hyperparameters; and, second, to indirectly benchmark against fairness-aware AutoML approaches, which attempt to train fair ML models by tuning the hyperparameters of unconstrained models [11, 23, 24].

**Unprocessing.** We define  $\pi_r(f)$  as the process of postprocessing a predictor  $f$  to minimize some classification loss function  $\ell$  over the group-specific decision thresholds  $t_s \in \mathbb{R}$ , subject to an  $r$ -relaxed equality of odds constraint (Equation 1),

$$\max_{y \in \{0,1\}} \left( \mathbb{P}[\hat{Y} = 1 | S = a, Y = y] - \mathbb{P}[\hat{Y} = 1 | S = b, Y = y] \right) \leq r, \quad \forall a, b \in \mathcal{S}, \quad (1)$$

where the prediction for a sample of group  $s \in \mathcal{S}$  is given by  $\hat{Y} = \mathbb{1}\{\hat{R} \geq t_s\}$ , and  $\hat{R}$  is its real-valued risk score. Thereby, *unprocessing* is defined as the unconstrained minimization of the loss  $\ell$ ; i.e.,  $\pi_\infty(f)$ , an  $\infty$ -relaxed solution to equality of odds. As classifiers with different values of constraint violation are potentially incomparable between themselves, *unprocessing* emerges as a means to fairer comparisons between classifiers. For example, while classifiers  $A$ ,  $B$ , and  $\hat{A}$  of Figure 2 are all Pareto-efficient [22] (i.e., incomparable), we can fairly compare the accuracy of  $A$  with  $\pi_\infty(B) = B^*$  (both are unconstrained classifiers),  $B$  with  $\pi_v(B) = \hat{B}$ , and  $\hat{A}$  with  $\pi_r(B)$ .

The following subsections will detail the datasets we use (Section 2.1), and the experimental procedure we employ to test our hypothesis (Section 2.2).

## 2.1 Datasets

We evaluate all methods on five large public benchmark datasets from the `folkttables` Python package [13]. These datasets are derived from the American Community Survey (ACS) public use microdata sample from 2018, containing a variety of demographic features (e.g., age, race, education).

Each of the five datasets is named after a specific prediction task: ACSIncome (1.6M rows) relates to household income prediction, ACSTravelTime (1.4M rows) relates to daily commute time prediction, ACSPublicCoverage (1.1M rows) relates to health insurance coverage prediction, ACSMobility (0.6M rows) relates to the prediction of address changes, and ACSEmployment (2.3M rows) relates to employment status prediction. ACSIncome arguably carries particular weight in the fair ML community, as it is a larger modern-day version of the popular UCI Adult dataset

(49K rows) [15], which has been widely used for benchmarking algorithmic fairness methods over the years. We use race group membership as the protected attribute on all five datasets (RAC1P column); specifically, we use samples from the four largest groups: *White*, *Black*, *Asian*, and *Other* (some other race alone). Additional experiments using only samples from the two largest groups are presented as well, although not the focus of the paper results’ analysis (see Appendix B). All fairness methods are trained to achieve equality of odds over members of different race groups — of course, standard unconstrained algorithms are blind to this constraint. In total, 10K models were trained and evaluated in the course of the paper’s experiments.

## 2.2 Experimental procedure

We conduct the following procedure for each dataset, with a 60%/20%/20% train/test/validation data split. First, we fit 1000 different ML models on the training data (50 per algorithm type). Second, to enable comparison of all models on an equal footing, we unprocess all 1000 trained models (on validation), and compute accuracy and equalized odds violation of the resulting classifiers. For any given classifier, its equalized odds violation (shown in plots as *constraint violation*) is given by the left-hand side of the inequality in Equation 1 (or, equivalently, the smallest slack  $r$  that fulfills the inequality). Then, we select the model with highest *unprocessed* accuracy,  $m^* = \pi_\infty(m')$ , obtained by the unconstrained postprocessing of the model  $m'$ . We defer the formal definition and procedure for solving the relaxed problem to Section 4.

We solve the  $r$ -relaxed equalized odds postprocessing on validation,  $\pi_r(m')$ , for all values of constraint violation,  $r \in [0, c(m^*)]$  (with discrete intervals of 0.01), where  $c(m^*)$  is the constraint violation of  $m^*$ . Finally, we compute accuracy and equalized odds violation on the withheld test dataset for all original 1000 models, and all post-processed versions of  $m'$ ,  $\pi_r(m')$ . All in all, even though the selection process for  $m^*$  and  $m'$  entirely disregarded fairness, we expect  $\pi_r(m')$  to be the classifier with highest accuracy at all levels of fairness  $r \in [0.0, 1.0]$  — as illustrated in Figure 2.

It may happen that the classifier  $m'$  with highest unprocessed accuracy is based on a pre- or unprocessing fairness method. Crucially, this implies that the means by which this fairness method resulted in a fairer classifier was by finding a more accurate classifier in the first place.

Figure 3 shows an example of the general effect of unprocessing on the ACSIncome dataset. On the left plots (original, unaltered models), the unconstrained (blue circles) and the LFR-based models (pink diamonds) are incomparable in terms of Pareto dominance between each other: the first is generally more accurate than the latter, but the ranking is reversed for constraint violation. However, after unprocessing all models (middle plots) we can see that unconstrained models are indeed better than LFR-based models, indicating that postprocessing the unconstrained models would be Pareto dominant over all LFR-based models. This is confirmed by the postprocessing curve of the unconstrained model  $A$  shown in the right plots. These conclusions hold on both RF- and GBM-based models, shown respectively on the top and bottom plots.

One final noteworthy point is that unconstrained models are not significantly affected by unprocessing, occupying approximately the same fairness-accuracy region before and after optimization over group-specific thresholds. This is expected, as unconstrained learning optimizes for calibration by group [19],  $P[Y = 1|R = r, S = s] = r, \forall s \in \mathcal{S}$ , which leads to the same loss-minimizing threshold for all groups,  $t_s = \frac{\ell(1,0)}{\ell(1,0) + \ell(0,1)}, \forall s \in \mathcal{S}$  (further details in Appendix D).

## 3 Results on American community survey data

In this section we will present and discuss the results of experiments on all five ACS / `folktables` datasets. These experiments entail a total of 1000 models trained per dataset. Due to space constraints, plots are shown only for the ACSIncome and ACSPublicCoverage datasets. Corresponding plots for

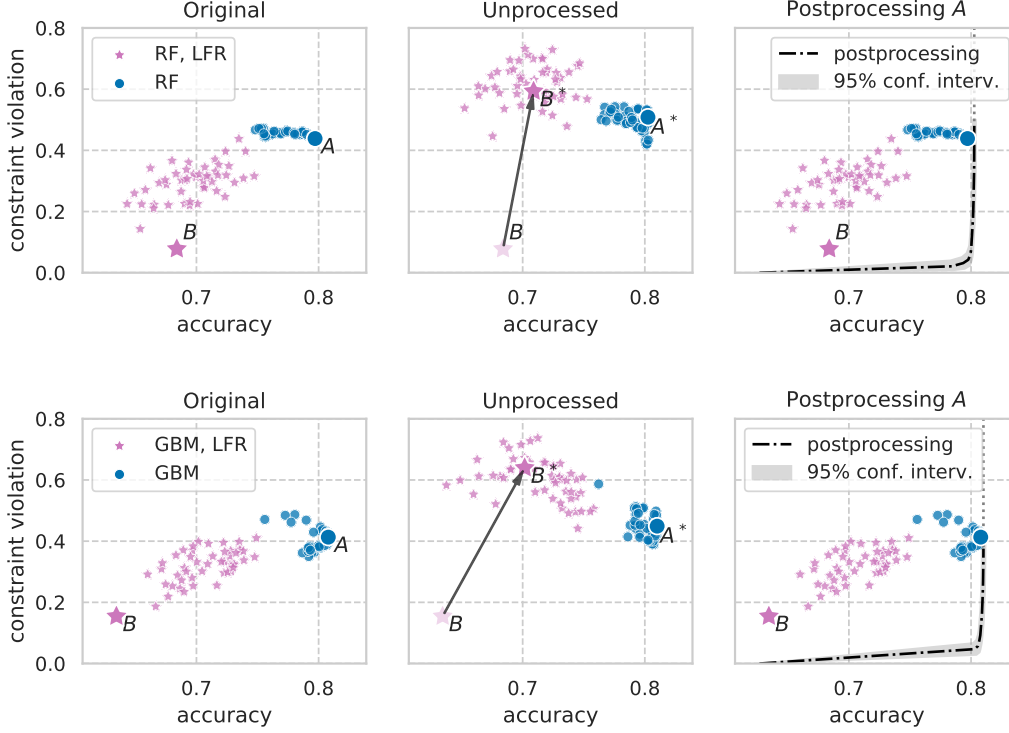


Figure 3: Real-data version of the illustrative plot shown in Figure 2 (results on ACSIncome test).  $A$  and  $B$  are two arbitrary incomparable models (both Pareto-efficient), which are made comparable after unprocessing. *Left plots*: original (unaltered) results; *Middle plots*: results after unprocessing all models; *Right plots*: original (unaltered) results, together with the postprocessing curve for the unconstrained model  $A$ .

the remaining datasets are shown in Appendix A. Results for a counterpart experiment using only two sensitive groups are also explored in this section, and further detailed in Appendix B.

### 3.1 Comparison between fairness methods

Although not the main focus of the paper, we first analyze how each fairness method compares with each other. Figure 4 shows the Pareto frontiers achieved by each method when paired with GBM models (see also Figure A1 of the appendix). Although LFR preprocessing (in pink) was consistently able to achieve some fairness improvement when compared with unconstrained models (in blue), these results are Pareto dominated by those attained by EG and FairGBM at most fairness levels. The CR preprocessing method (in yellow) was Pareto dominated at all levels of fairness on 3 out of 5 datasets, and overall achieved lackluster results on all datasets.

Interestingly, inprocessing fairness methods were able to achieve higher accuracy than the unconstrained GBM models. Figure 5 shows one potential reason: inprocessing fairness methods can take notoriously high compute resources to train, potentially giving them a compute advantage with respect to their unconstrained counterparts. While all methods in the comparison are given the same number of random hyperparameter search trials ( $n = 50$ ), the EG inprocessing method essentially relies on ensembling the base GBM model, dramatically increasing its training time but also expectedly reducing the model’s variance and hence improving its performance [6, 20].

All in all, preprocessing methods (CR and LFR) performed worst (lowest area within respective Pareto frontiers), while the EG and FairGBM inprocessing methods performed best.



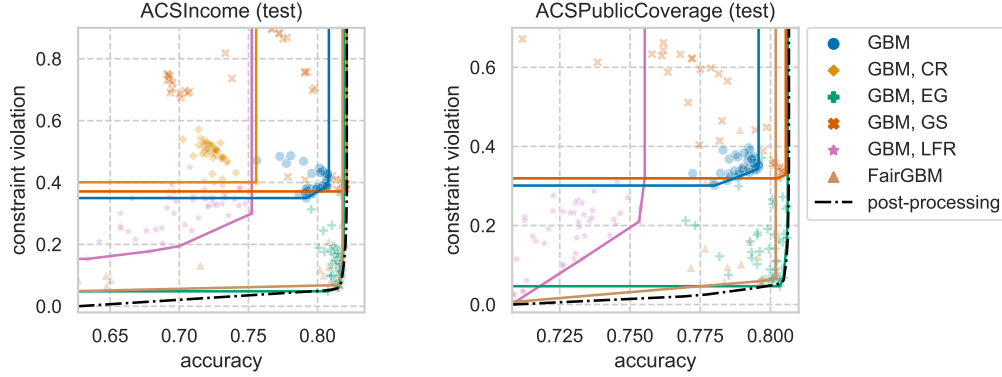


Figure 4: Pareto frontier attained by each GBM-based algorithm, together with the Pareto frontier attained by postprocessing the GBM-based model with highest unprocessed validation accuracy,  $m^*$ . On ACSPublicCoverage (right), the  $\langle \text{GBM}, \text{CR} \rangle$  Pareto frontier is fully outside the shown region (towards inferior results).

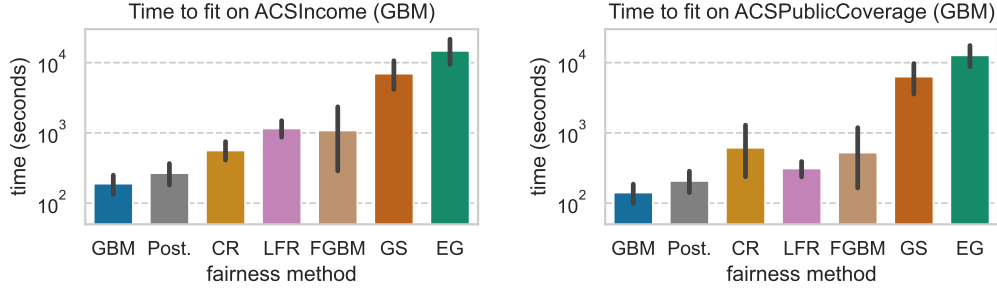


Figure 5: Mean time to fit the base GBM model and each studied fairness method on the ACSIncome (left plot) and ACSPublicCoverage (right plot) datasets, with 95% confidence intervals (dark lines). Note the  $\log$  scale: the EG inprocessing method takes, on average, 78 times longer and 90 times longer to fit than the base GBM model, respectively on ACSIncome and ACSPublicCoverage.

### 3.2 Postprocessing vs other methods

Figure 6 (as well as Figures A2–A5 of the appendix) shows test-set results for the experimental procedure detailed in Section 2.2. The model with highest unprocessed validation accuracy,  $m^*$ , is shown with a larger marker, and its postprocessing Pareto frontier is shown with a black dash-dot line. Figures A8–A12 of the appendix show a similar plot on a subset of models (only GBM-based models), with an identical trend.

All datasets show a wide spread of models throughout the fairness-accuracy space, although to varying levels of maximum accuracy for each ACS dataset (from 0.706 on ACSTravelTime to 0.832 on ACSEmployment). On the ACSPublicCoverage, ACSIncome, and ACSEmployment datasets, the  $m^*$  model is of type  $\langle \text{GBM}, \text{EG} \rangle$  (blue plus marker). On ACSTravelTime, the  $m^*$  model is of type  $\langle \text{GBM}, \text{GS} \rangle$ . ACSMobility is the only dataset where  $m^*$  is not GBM-based, being of type  $\langle \text{RF}, \text{GS} \rangle$  instead (orange cross marker). On the ACSPublicCoverage dataset, unconstrained models (circles) are found around the 0.35 constraint violation mark, similarly to the unprocessed optimum model.

Crucially, on all studied datasets, postprocessing the most accurate model resulted in the fair optima for all values of fairness constraint violation, either dominating or matching other contender models (within 95% confidence intervals).

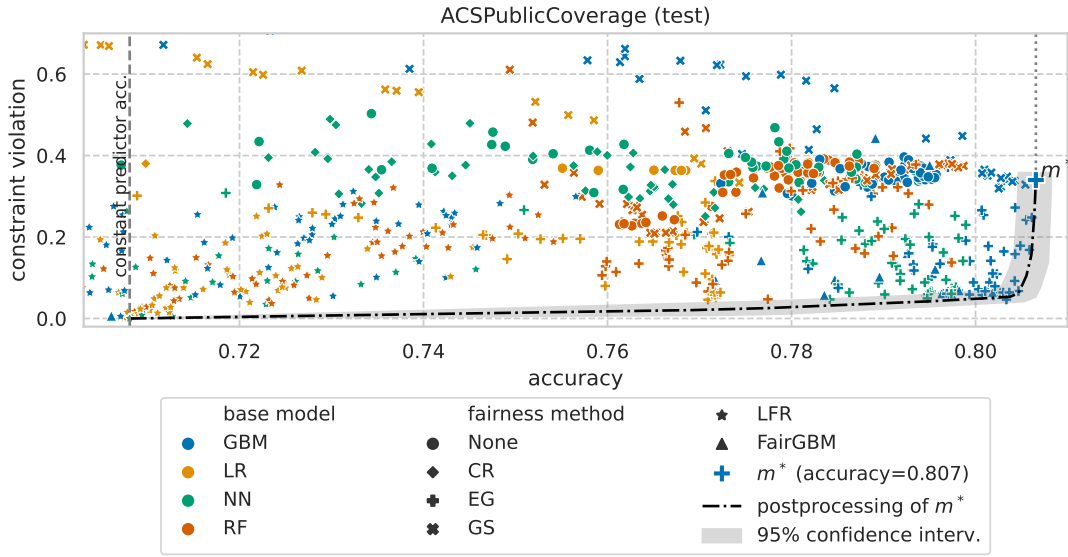


Figure 6: Fairness and accuracy test results for all 1000 trained ML models (50 of each type) on the ACSPublicCoverage dataset. Colors portray different underlying unconstrained models and markers portray different fairness methods (or no fairness method for circle markers). The model with highest unprocessed validation accuracy,  $m^*$ , is shown with a larger marker (blue plus), and the Pareto frontier attainable by postprocessing  $m^*$  is shown as a black dash-dot line.

Figure 7 shows a zoom on the bottom right portion of the larger plots (together with Figures A6–A7). Neither preprocessing methods nor LR-based method manage to be inside the zoomed-in plots. On all datasets, there is a variety of models that do match the postprocessing of  $m^*$  (within the 95% confidence intervals). These models also achieved unprocessed accuracy values that were competitive with  $m^*$ , and would expectedly have similar postprocessing curves.

Finally, Figure 8 portrays results for a different experiment — a different set of 5K trained models — with fairness constraints measured only on the two largest sub-groups (*White* and *Black*). This leads to an arguably easier problem to solve, which is reflected on the general compression of models on the vertical axis (reduced constraint violation). While previously the maximum unprocessed accuracy on ACSIncome was achieved at 39% constraint violation, on this binary-group setting it is achieved at 19% constraint violation. Nonetheless, the postprocessing Pareto frontier still dominates or matches the remaining fairness methods. The same trend is visible on all studied datasets.

All in all, postprocessing provides a full view of the Pareto frontier, derived from a single predictor  $m^*$ . Regardless of fairness violation, when this predictor is near-optimal — potentially achievable on tabular data by training a variety of algorithms — so will the postprocessed Pareto frontier be.

## 4 Achieving relaxed error rate parity

Error rate parity, also known as equalized odds, enforces equal false positive rate (FPR) and equal true positive rate (TPR) between different protected groups [16]. This can be formalized as a constraint on the joint distribution of  $(Y, \hat{Y}, S)$ :

$$\mathbb{P}[\hat{Y} = 1 | S = a, Y = y] = \mathbb{P}[\hat{Y} = 1 | S = b, Y = y], \quad \forall y \in \{0, 1\}, \quad \forall a, b \in \mathcal{S}, \quad (2)$$

where  $a \neq b$  references two distinct groups in the set of all possible groups  $\mathcal{S}$ .



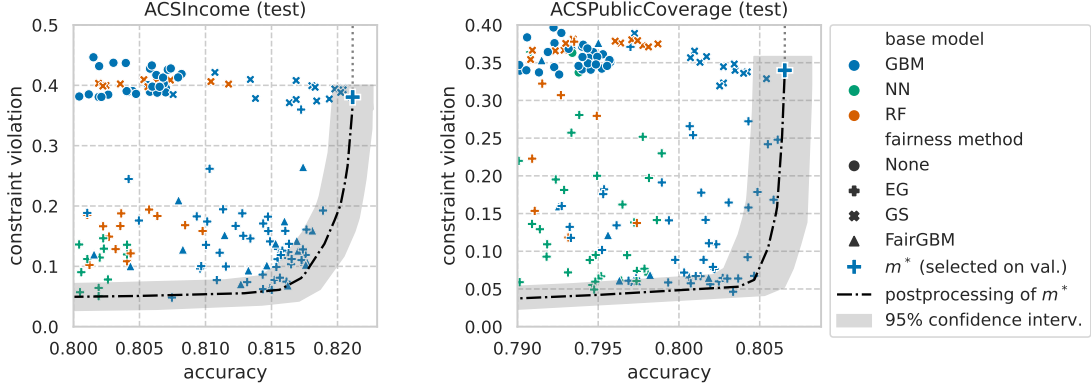


Figure 7: Detailed look at the postprocessing Pareto frontier on the ACSIncome (left) and ACSPublicCoverage (right) datasets. As shown, postprocessing  $m^*$  dominates or matches all 1000 trained ML models, regardless of the underlying train algorithm (preprocessing, inprocessing, or unconstrained).

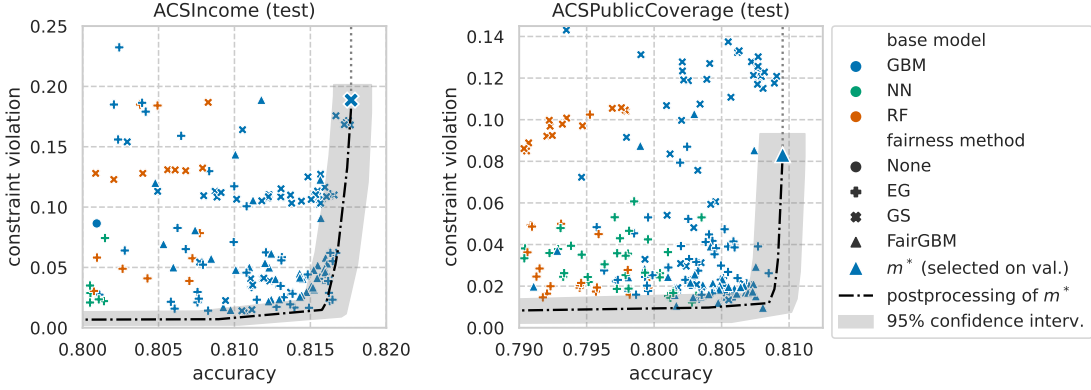


Figure 8: **[Binary protected groups]** Results for a counterpart to the main experiment, in which only samples from the two largest groups are used (*White* and *Black*). This significantly reduces the *measured* disparities: note the reduced  $y$  axis range when compared with Figure 7.

Fulfilling the strict equalized odds constraint greatly simplifies the optimization problem of finding the optimal classifier through postprocessing, as the constrained optimum must be at the intersection of the convex hulls of each group-specific ROC curve. As such, we're left with a linear optimization problem on a single 2-dimensional variable,  $\gamma = (\gamma_0, \gamma_1)$ :

$$\min_{\gamma \in D} \gamma_0 \cdot \ell(1, 0) \cdot p_0 + (1 - \gamma_1) \cdot \ell(0, 1) \cdot p_1, \quad (3)$$

where  $\gamma_0$  is the global FPR,  $\gamma_1$  the global TPR,  $D \subset [0, 1]^2$  the optimization domain,  $p_y = \mathbb{P}[Y = y]$  the prevalence of label  $Y = y$ , and  $\ell(\hat{y}, y)$  the loss incurred for predicting  $\hat{y}$  when the correct class was  $y$  (we assume w.l.o.g.  $\ell(0, 0) = \ell(1, 1) = 0$ ). Moreover, strict equal odds fulfillment collapses the optimization domain  $D$  into a single convex polygon that results from intersecting all group-specific ROC hulls; i.e.,  $D = \bigcap_{s \in \mathcal{S}} D_s$ , where  $D_s$  is the convex hull of the ROC curve for group  $s$ . Specifically,  $D_s = \text{convexhull} \{C_s(t) : t \in \mathbb{R}\}$ , and  $C_s$  defines the ROC curve for group  $s$  as:

$$C_s(t) = \left( \mathbb{P} \left[ \hat{R} \geq t | S = s, Y = 0 \right], \mathbb{P} \left[ \hat{R} \geq t | S = s, Y = 1 \right] \right), \quad (4)$$

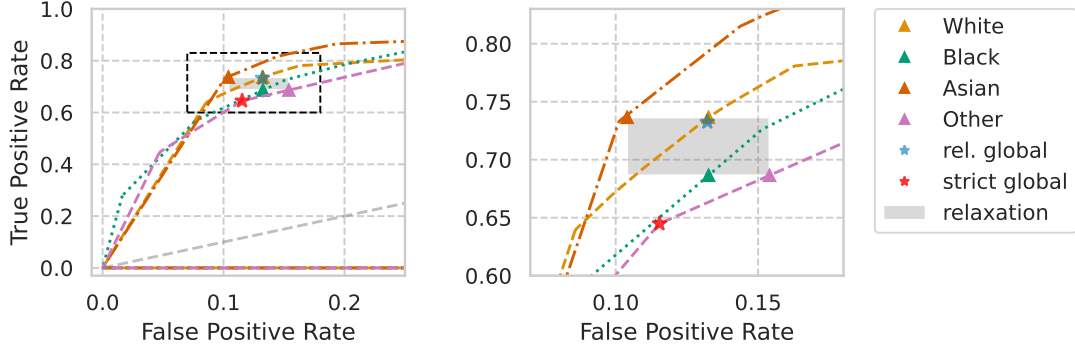


Figure 9: Optimal solution to a strict (red star) and a 0.05-relaxed (blue star) equalized odds constraint. Right plot shows a zoom on the region of interest (represented by dashed black rectangle).

where  $t \in \mathbb{R}$  is a group-specific decision threshold, and  $\hat{R}$  is the predictor’s real-valued score.

In this section, we detail the solution to the  $r$ -relaxed equalized odds constraint defined in Equation 1. In order to relax the equalized odds constraint, we introduce a slack variable,  $\delta^{(a,b)} \in [0, 1]^2$ , for each pair  $a, b \in \mathcal{S}$ :

$$\mathbb{P}[\hat{Y} = 1 | S = a, Y = y] - \mathbb{P}[\hat{Y} = 1 | S = b, Y = y] = \delta_y^{(a,b)} \leq r, \quad (5)$$

where  $r \in [0, 1]$  is the maximum allowed constraint violation.

We introduce variables  $\gamma^{(s)} = (\gamma_0^{(s)}, \gamma_1^{(s)}) \in D_s, s \in \mathcal{S}$ , as the points of group-specific FPR,  $\gamma_0^{(s)}$ , and group-specific TPR,  $\gamma_1^{(s)}$ . Equation 5 can then be equivalently stated as:

$$\left\| \gamma^{(a)} - \gamma^{(b)} \right\|_{\infty} = \left\| \delta^{(a,b)} \right\|_{\infty} \leq r. \quad (6)$$

The global ROC point,  $\gamma$ , is defined as:

$$\gamma_0 = \sum_{s \in \mathcal{S}} \gamma_0^{(s)} \cdot p_{s|0}, \quad \gamma_1 = \sum_{s \in \mathcal{S}} \gamma_1^{(s)} \cdot p_{s|1}, \quad (7)$$

where  $p_{s|y} = \mathbb{P}[S = s | Y = y]$  is the relative size of group  $s$  within the set of samples with label  $Y = y$ . Importantly, the global point  $\gamma$  is not limited to the intersection of group-specific ROC hulls. Each group-specific ROC point is naturally limited to be inside its group-specific ROC hull,  $\gamma^{(s)} \in D_s$ , and  $\gamma$  is only limited by its definition as a function of all  $\gamma^{(s)}, s \in \mathcal{S}$ , as per Equation 7.

Finally, finding the  $r$ -relaxed optimum boils down to solving Equation 3 with domain  $D = \bigcup_{s \in \mathcal{S}} D_s$ , subject to constraints defined in Equations 6–7.

As  $\ell_{\infty}$  inequality constraints are convex, and the objective function linear, this optimization problem amounts to a linear program (LP), for which there is a variety of efficient open-source solvers [12]. We contribute a solution to the relaxed equality of odds constraint, and open-source the implementation in an easy to use Python package.<sup>1</sup>

Figure 9 shows an example of optimal strict and 0.05-relaxed solutions for equality of odds. The computed ROC convex hulls correspond to the predictions of a GBM model on the ACSIncome dataset, for each of the four largest groups. Strict fulfillment of the equality of odds constraint (red star) reduces the feasible space of solutions to the intersection of all group-specific ROC hulls. This fact potentially restricts all but one group to sub-optimal accuracy, achieved by randomizing some portion of the classifier’s predictions. On the other hand, if we allow for some relaxation of the constraint, each group’s ROC point will lie closer to its optimum. In this example, the optimal solution to an  $r = 0.05$  relaxation is no longer forced to randomize part of the classifier’s predictions, placing each group’s ROC point on the frontier of its ROC convex hull.

## Acknowledgments

We’re indebted to Noam Barda, Noa Dagan, and Guy Rothblum for insightful and stimulating discussions about the project.

## References

- [1] Alekh Agarwal, Alina Beygelzimer, Miroslav Dudík, John Langford, and Hanna Wallach. A reductions approach to fair classification. In *International Conference on Machine Learning*, pages 60–69, 2018.
- [2] Julia Angwin, Jeff Larson, Lauren Kirchner, and Surya Mattu. Machine bias: There’s software used across the country to predict future criminals. and it’s biased against blacks. <https://www.propublica.org/article/machine-bias-risk-assessments-in-criminal-sentencing>, May 2016.
- [3] Michelle Bao, Angela Zhou, Samantha Zottola, Brian Brubach, Brian Brubach, Sarah Desmarais, Aaron Horowitz, Kristian Lum, and Suresh Venkatasubramanian. It’s compaslicated: The messy relationship between RAI datasets and algorithmic fairness benchmarks. In Joaquin Vanschoren and Sai-Kit Yeung, editors, *Proceedings of the Neural Information Processing Systems Track on Datasets and Benchmarks 1, NeurIPS Datasets and Benchmarks 2021, December 2021, virtual*, 2021.
- [4] Solon Barocas, Moritz Hardt, and Arvind Narayanan. *Fairness and Machine Learning: Limitations and Opportunities*. fairmlbook.org, 2019. <http://www.fairmlbook.org>.
- [5] Sarah Bird, Miro Dudík, Richard Edgar, Brandon Horn, Roman Lutz, Vanessa Milan, Mehrnoosh Sameki, Hanna Wallach, and Kathleen Walker. Fairlearn: A toolkit for assessing and improving fairness in AI. Technical Report MSR-TR-2020-32, Microsoft, May 2020.
- [6] Leo Breiman. Bagging predictors. *Machine learning*, 24:123–140, 1996.
- [7] L. Elisa Celis, Lingxiao Huang, Vijay Keswani, and Nisheeth K. Vishnoi. Classification with fairness constraints: A meta-algorithm with provable guarantees. In *Proceedings of the Conference on Fairness, Accountability, and Transparency, FAT\* ’19*, page 319–328, New York, NY, USA, 2019. Association for Computing Machinery.
- [8] Sam Corbett-Davies, Emma Pierson, Avi Feller, Sharad Goel, and Aziz Huq. Algorithmic decision making and the cost of fairness. In *Proceedings of the 23rd acm sigkdd international conference on knowledge discovery and data mining*, pages 797–806, 2017.
- [9] Andrew Cotter, Heinrich Jiang, Serena Wang, Taman Narayan, Seungil You, Karthik Sridharan, and Maya R. Gupta. Optimization with non-differentiable constraints with applications to fairness, recall, churn, and other goals. *Journal of Machine Learning Research*, 2019.
- [10] André F. Cruz, Catarina Belém, João Bravo, Pedro Saleiro, and Pedro Bizarro. FairGBM: Gradient boosting with fairness constraints. In *The Eleventh International Conference on Learning Representations*, 2023.
- [11] André F. Cruz, Pedro Saleiro, Catarina Belém, Carlos Soares, and Pedro Bizarro. Promoting fairness through hyperparameter optimization. In *2021 IEEE International Conference on Data Mining (ICDM)*, pages 1036–1041, 2021.
- [12] Steven Diamond and Stephen Boyd. CVXPY: A Python-embedded modeling language for convex optimization. *Journal of Machine Learning Research*, 17(83):1–5, 2016.

- [13] Frances Ding, Moritz Hardt, John Miller, and Ludwig Schmidt. Retiring adult: New datasets for fair machine learning. In *Advances in Neural Information Processing Systems*, volume 34, pages 6478–6490, 2021.
- [14] Michele Donini, Luca Oneto, Shai Ben-David, John S Shawe-Taylor, and Massimiliano Pontil. Empirical risk minimization under fairness constraints. In *Advances in Neural Information Processing Systems*, volume 31, 2018.
- [15] Dheeru Dua and Casey Graff. UCI Machine Learning Repository, 2017.
- [16] Moritz Hardt, Eric Price, and Nathan Srebro. Equality of opportunity in supervised learning. In D. Lee, M. Sugiyama, U. Luxburg, I. Guyon, and R. Garnett, editors, *Advances in Neural Information Processing Systems*, volume 29. Curran Associates, Inc., 2016.
- [17] Ben Hutchinson and Margaret Mitchell. 50 years of test (un) fairness: Lessons for machine learning. In *Proceedings of the conference on fairness, accountability, and transparency*, pages 49–58, 2019.
- [18] Maximilian Kasy and Rediet Abebe. Fairness, equality, and power in algorithmic decision-making. In *Proceedings of the 2021 ACM Conference on Fairness, Accountability, and Transparency*, pages 576–586, 2021.
- [19] Lydia T. Liu, Max Simchowitz, and Moritz Hardt. The implicit fairness criterion of unconstrained learning. In Kamalika Chaudhuri and Ruslan Salakhutdinov, editors, *Proceedings of the 36th International Conference on Machine Learning*, volume 97 of *Proceedings of Machine Learning Research*, pages 4051–4060. PMLR, 09–15 Jun 2019.
- [20] Richard Maclin and David Opitz. An empirical evaluation of bagging and boosting. *AAAI/IAAI*, 1997:546–551, 1997.
- [21] Aditya Krishna Menon and Robert C Williamson. The cost of fairness in binary classification. In *Conference on Fairness, accountability and transparency*, pages 107–118. PMLR, 2018.
- [22] Vilfredo Pareto. *Manuale di economia politica: con una introduzione alla scienza sociale*, volume 13. Società editrice libraria, 1919.
- [23] Valerio Perrone, Michele Donini, Muhammad Bilal Zafar, Robin Schmucker, Krishnaram Kenthapadi, and Cédric Archambeau. Fair bayesian optimization. In *Proceedings of the 2021 AAAI/ACM Conference on AI, Ethics, and Society*, AIES ’21, page 854–863, New York, NY, USA, 2021. Association for Computing Machinery.
- [24] Hilde Weerts, Florian Pfisterer, Matthias Feurer, Katharina Eggenberger, Edward Bergman, Noor Awad, Joaquin Vanschoren, Mykola Pechenizkiy, Bernd Bischl, and Frank Hutter. Can fairness be automated? guidelines and opportunities for fairness-aware automl. *arXiv preprint arXiv:2303.08485*, 2023.
- [25] Blake Woodworth, Suriya Gunasekar, Mesrob I Ohannessian, and Nathan Srebro. Learning non-discriminatory predictors. In *Conference on Learning Theory*, pages 1920–1953. PMLR, 2017.
- [26] Muhammad Bilal Zafar, Isabel Valera, Manuel Gomez-Rodriguez, and Krishna P Gummadi. Fairness constraints: A flexible approach for fair classification. *The Journal of Machine Learning Research*, 20(1):2737–2778, 2019.
- [27] Rich Zemel, Yu Wu, Kevin Swersky, Toni Pitassi, and Cynthia Dwork. Learning fair representations. In *International Conference on Machine Learning*, pages 325–333, 2013.

## A Additional experimental results

The main body of the paper discusses results on all five `folktables` datasets. However, due to space constraints, particular focus is given to results on two example datasets: `ACSIIncome` and `ACSPublicCoverage`. This section shows analogous versions of each previously shown plot for the remaining three studied datasets: `ACSTravelTime`, `ACSMobility`, and `ACSEmployment`.

### A.1 Comparison between fairness methods

Figure A1 shows Pareto frontiers for all studied GBM-based algorithms. We observe a similar trend to that seen in Figure 4: preprocessing fairness methods can increase fairness but at dramatic accuracy costs, while EG and FairGBM inprocessing fairness methods trade Pareto-dominance between each other. Postprocessing Pareto frontier is also shown for reference, but a more detailed comparison between postprocessing and all other contender models will be shown in the following section.

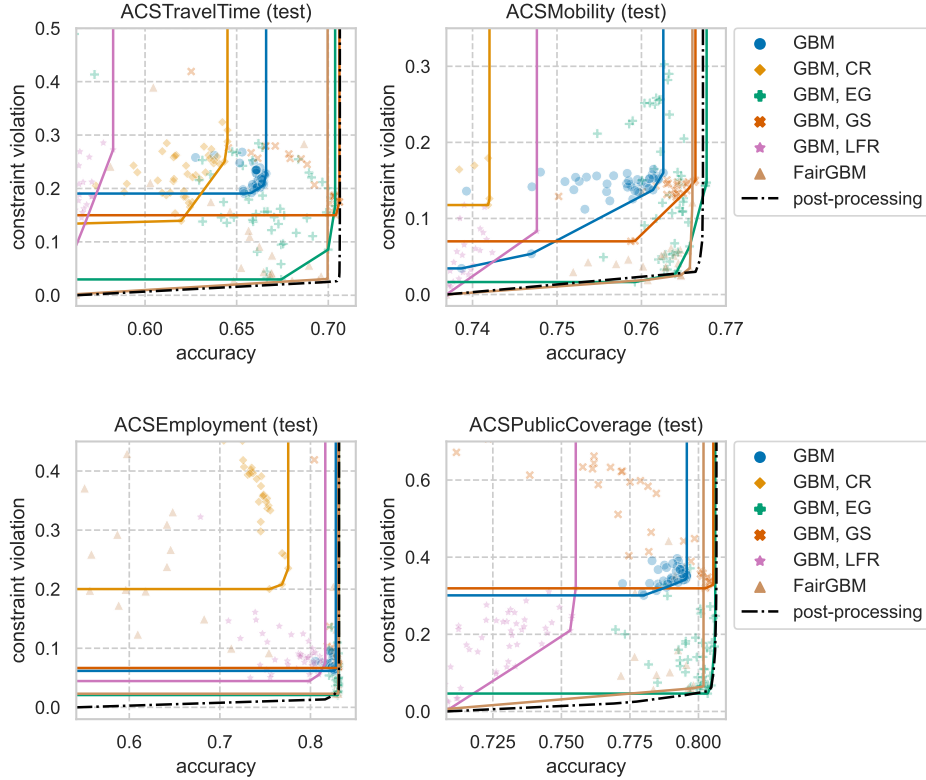


Figure A1: Pareto frontier attainable by each GBM-based ML algorithm, together with the Pareto frontier attained by postprocessing  $m^*$ , the GBM-based model with highest unprocessed accuracy (on validation). Plotted Pareto curves are linearly interpolated between Pareto-efficient models.

### A.2 Postprocessing vs other methods

Figures A2–A5 show complete views of the Pareto frontier obtained by postprocessing each dataset’s  $m^*$  model, together with a scatter of all other competing preprocessing, inprocessing, or unconstrained models (1000 in total per dataset). Figures A6–A7 show detailed postprocessing results on each

dataset, zoomed on the region of interest (maximal accuracy and minimal constraint violation, i.e., bottom right portion of the plot). The main paper hypothesis is confirmed on each dataset: we can obtain optimally fair classifiers at any level of constraint violation by postprocessing the model with highest accuracy,  $m^*$ , irrespective of its constraint violation.

Figures A8–A12 show results using only a subset of models: only GBM-based models. On the ACSMobility dataset, we can see the postprocessing frontiers attained by two different models: the first of type  $\langle \text{RF}, \text{GS} \rangle$  (Figure A4), and the second of type  $\langle \text{GBM}, \text{EG} \rangle$  (Figure A11). Although the RF-based model was selected as  $m^*$  among all models, the differences in unprocessed validation accuracy between the two models were not statistically significant. That is, both models could be selected with similar expected postprocessing results, as confirmed by comparing the plotted postprocessing frontiers of each model.

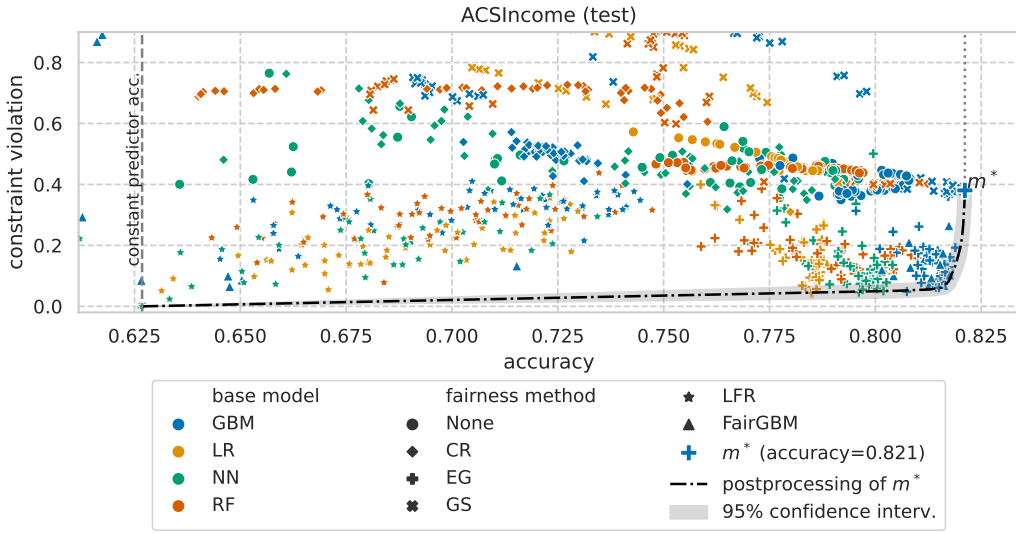


Figure A2: Fairness and accuracy test results for all 1000 trained ML models (50 of each type) on the ACSIncome dataset, together with the Pareto frontier attained by postprocessing  $m^*$ . This is a colored and more detailed version of Figure 1. See caption of Figure 6 for further details.

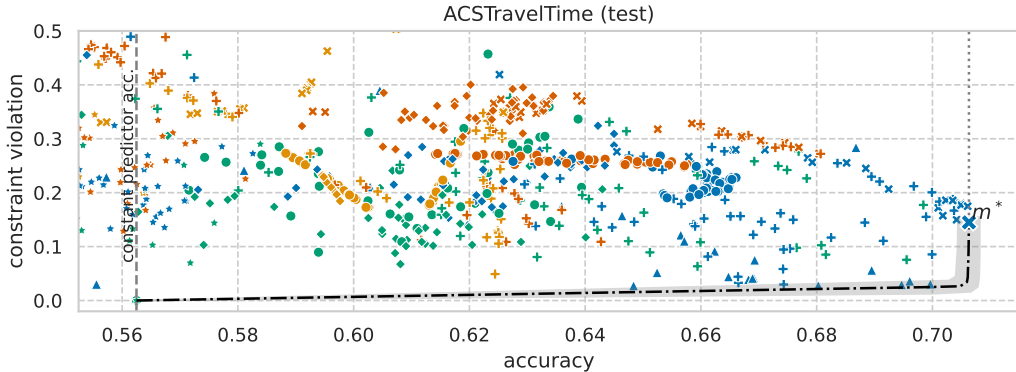


Figure A3: Fairness and accuracy test results on the ACSTravelTime dataset. The same legend as Figure A2 is used, except  $m^*$  is of type  $\langle \text{GBM}, \text{GS} \rangle$  and achieves 0.706 accuracy.



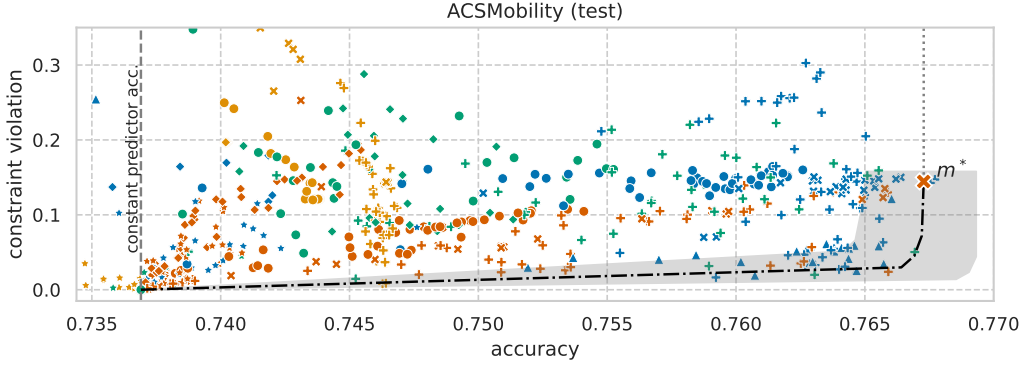


Figure A4: Fairness and accuracy test results on the ACSMobility dataset. The same legend as Figure A2 is used, except  $m^*$  is of type (RF, GS) and achieves 0.767 accuracy.

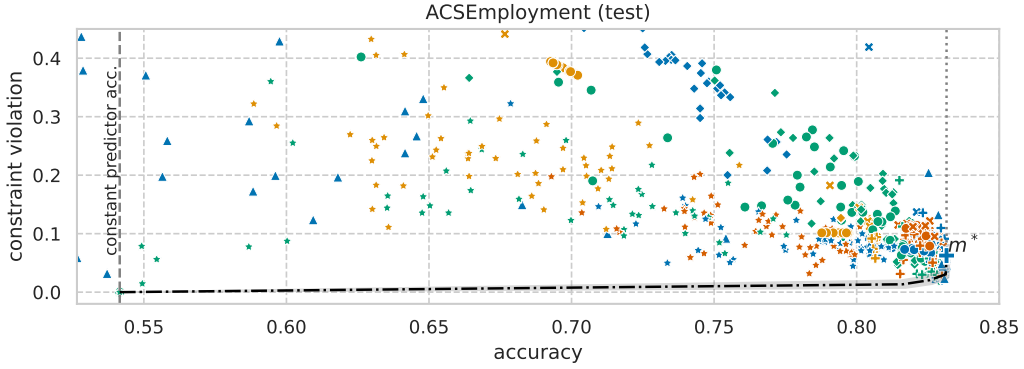


Figure A5: Fairness and accuracy test results on the ACSEmployment dataset. The same legend as Figure A2 is used, except  $m^*$  is of type (GBM, EG) and achieves 0.832 accuracy).

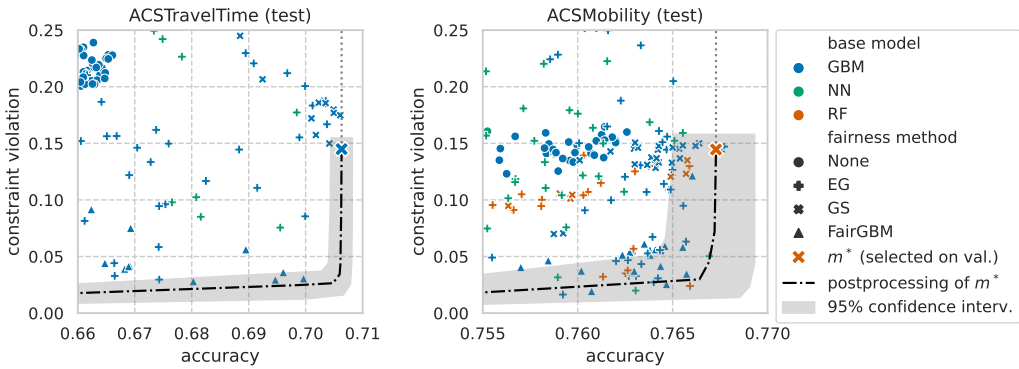


Figure A6: Detailed view of the postprocessing Pareto frontier on the ACSTravelTime (left) and ACSMobility (right) datasets. Corresponds to zoomed-in versions of Figures A3 (left) and A4 (right).

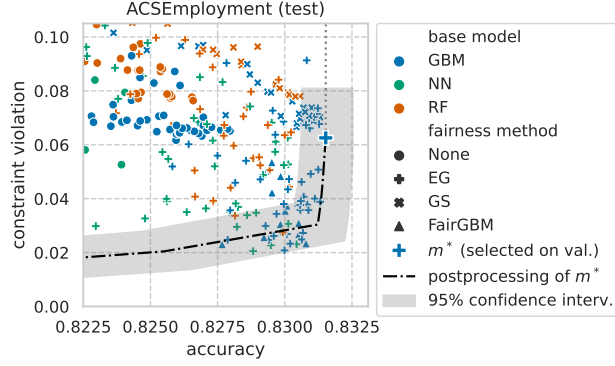


Figure A7: Detailed view of the postprocessing Pareto frontier on the ACSEmployment dataset. Corresponds to a zoomed-in version of Figure A5.

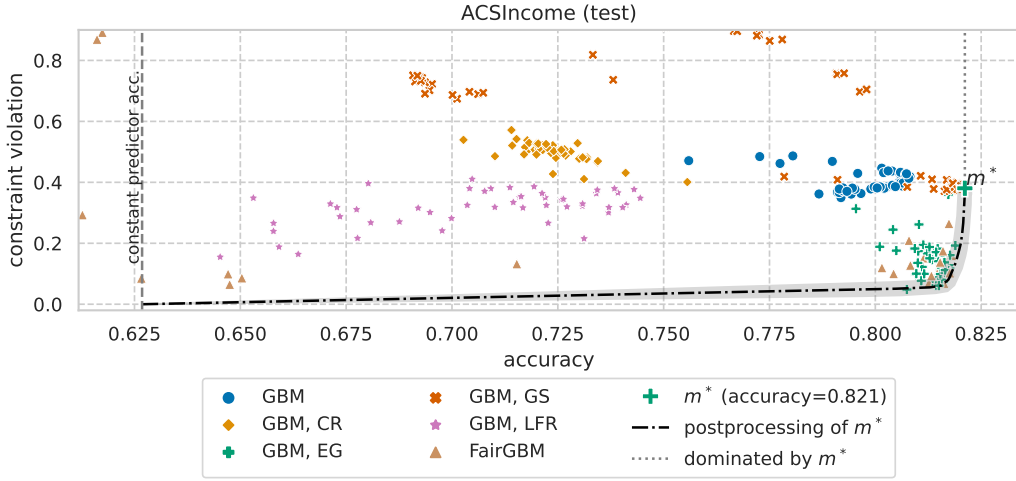


Figure A8: Fairness and accuracy test results for 300 GBM-based ML models (50 of each algorithm type) on the ACSIncome dataset. The model with highest validation accuracy,  $m^*$ , is shown with a larger marker, and the Pareto frontier attainable by postprocessing  $m^*$  is shown as a black dash-dot line.

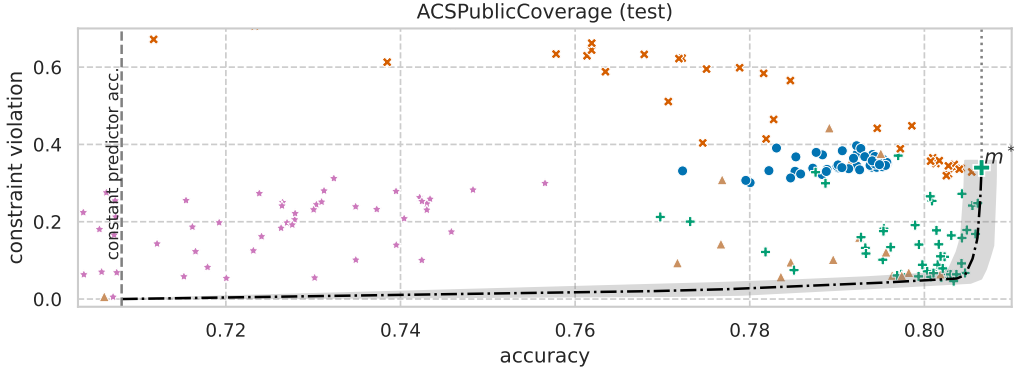


Figure A9: Fairness and accuracy test results for GBM-based ML models on the ACSPublicCoverage dataset.

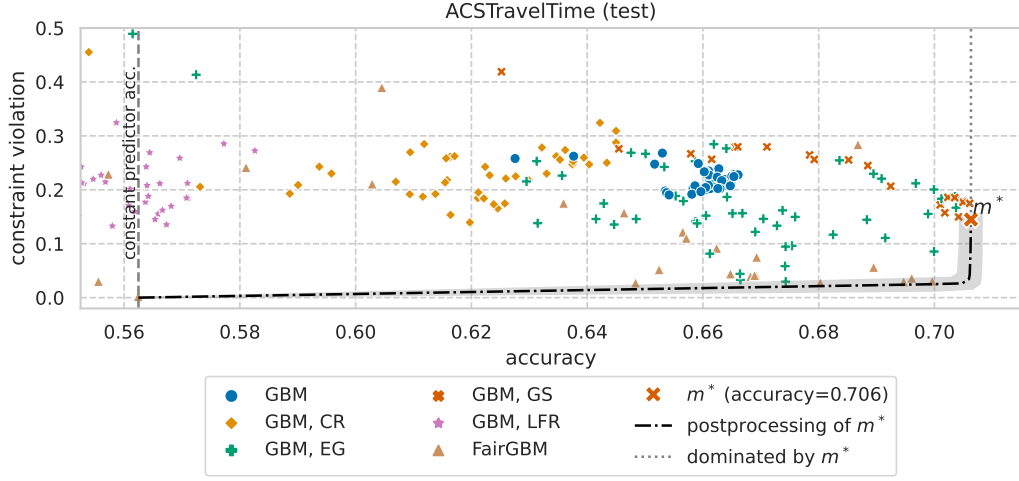


Figure A10: Fairness and accuracy test results for GBM-based ML models on the ACSTravelTime dataset.

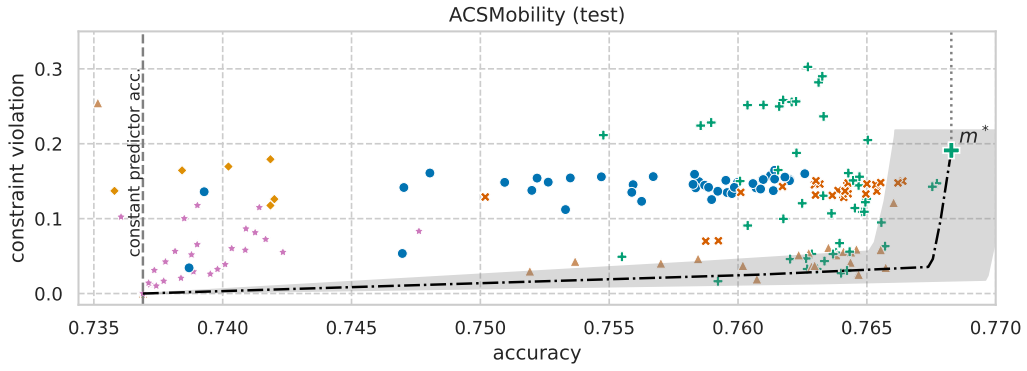


Figure A11: Fairness and accuracy test results for GBM-based ML models on the ACSMobility dataset.

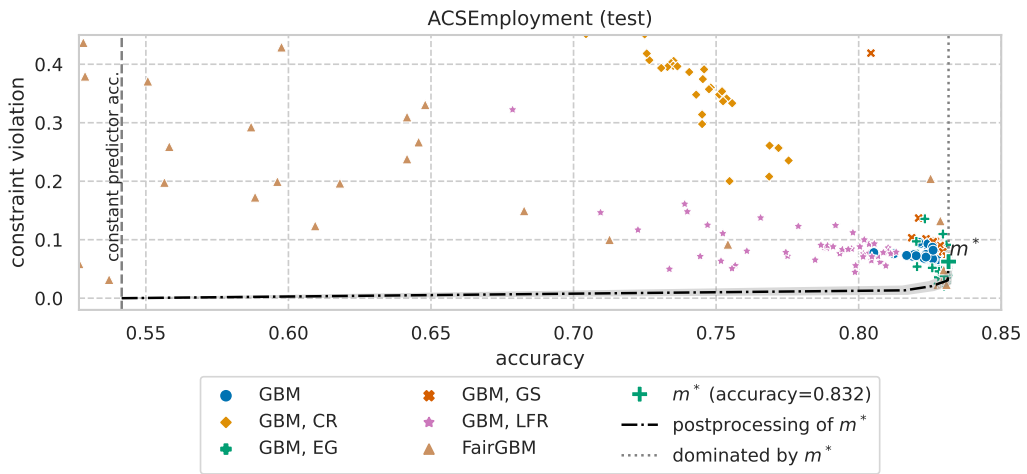


Figure A12: Fairness and accuracy test results for GBM-based ML models on the ACSEmployment dataset.

### A.3 Time to fit each method

Figure A13 shows the mean time to fit each GBM-based model on three separate datasets. The trend is clear on all studied datasets: postprocessing is a small increment to the time taken to fit the base model, preprocessing methods take longer but are still within the same order of magnitude, the FairGBM inprocessing method also incurs a relatively small increment to the base model time, while EG and GS take one to two orders of magnitude longer to fit.

For clarification, all times listed are end-to-end process times for fitting and evaluating a given model. For example, postprocessing times include the time taken to fit the base GBM model plus the time taken to solve the LP. Likewise, preprocessing fairness methods include the time taken to fit the preprocessing method, the time taken to transform the input data, and the time to fit the base GBM model. Finally, inprocessing fairness methods include the time taken to fit the inprocessing method, as no preprocessing or postprocessing steps are required. Nonetheless, the GS and EG inprocessing methods take significantly longer than any other competing method.

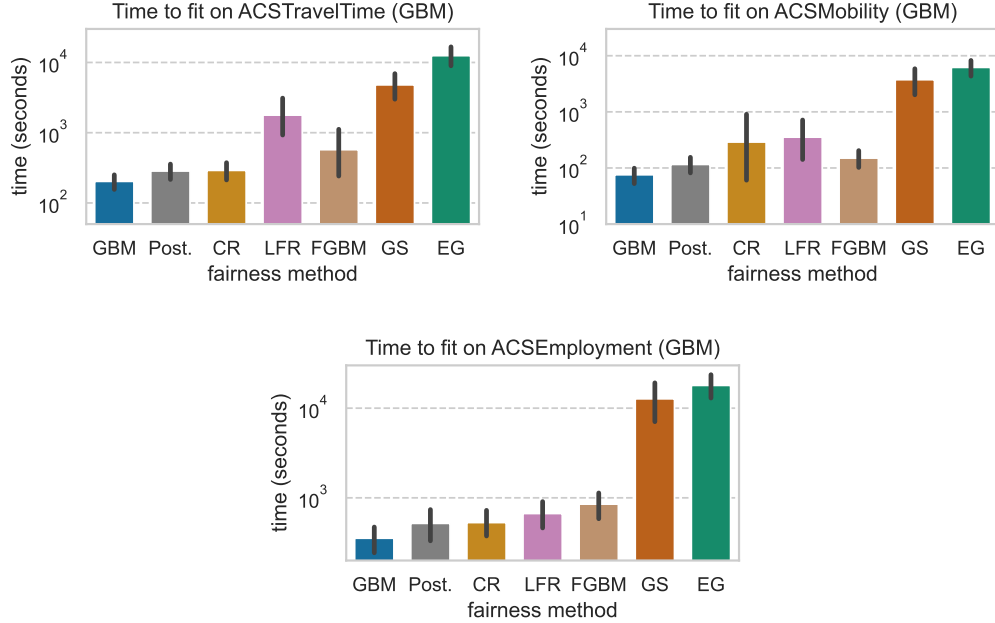


Figure A13: Mean time to fit the base GBM model and each studied fairness method on ACSTravelTime (left), ACSMobility (right), and ACSEmployment (bottom), with 95% confidence intervals.

## B Experiments with binary sensitive groups

While compatibility with more than two sensitive groups is arguably essential for real-world applicability of a fairness intervention, it is common among the fair ML literature to evaluate methods using only two sensitive groups [27, 1, 10].

In this binary-group setting, constrained optimization methods only have to consider two constraints:

$$\begin{aligned}
 \left| \mathbb{P} \left[ \hat{Y} = 1 | S = 0, Y = 0 \right] - \mathbb{P} \left[ \hat{Y} = 1 | S = 1, Y = 0 \right] \right| &\leq \epsilon, &> \text{FPR constraint} \\
 \left| \mathbb{P} \left[ \hat{Y} = 1 | S = 0, Y = 1 \right] - \mathbb{P} \left[ \hat{Y} = 1 | S = 1, Y = 1 \right] \right| &\leq \epsilon, &> \text{TPR constraint}
 \end{aligned}$$

respectively, a constraint on group-specific FPR, and another on group-specific TPR, with some small  $\epsilon$  slack. This leads to an overall easier equalized odds problem, both from the reduced number of constraints, as well as the naturally lower observed constraint violation. By making the equalized odds constraint easier to fulfill, we expect to provide fairness methods with the best chance at disproving the paper hypothesis.

Figure A14 (as Figure 8) shows results of applying the experimental procedure detailed in Section 2.2 to a sub-sample of the ACS / folktables datasets: only samples from the two largest sensitive groups are used (*White* and *Black*). We observe considerably lower constraint violation across the board, both for unconstrained and fairness-aware models. In fact, even unconstrained unprocessed models ( $m^*$  on each plot) achieve below 0.1 constraint violation on 4 datasets when using binary groups (all but ACSIncome), and below 0.03 on 2 datasets (ACSMobility and ACSEmployment, see Figure A14).

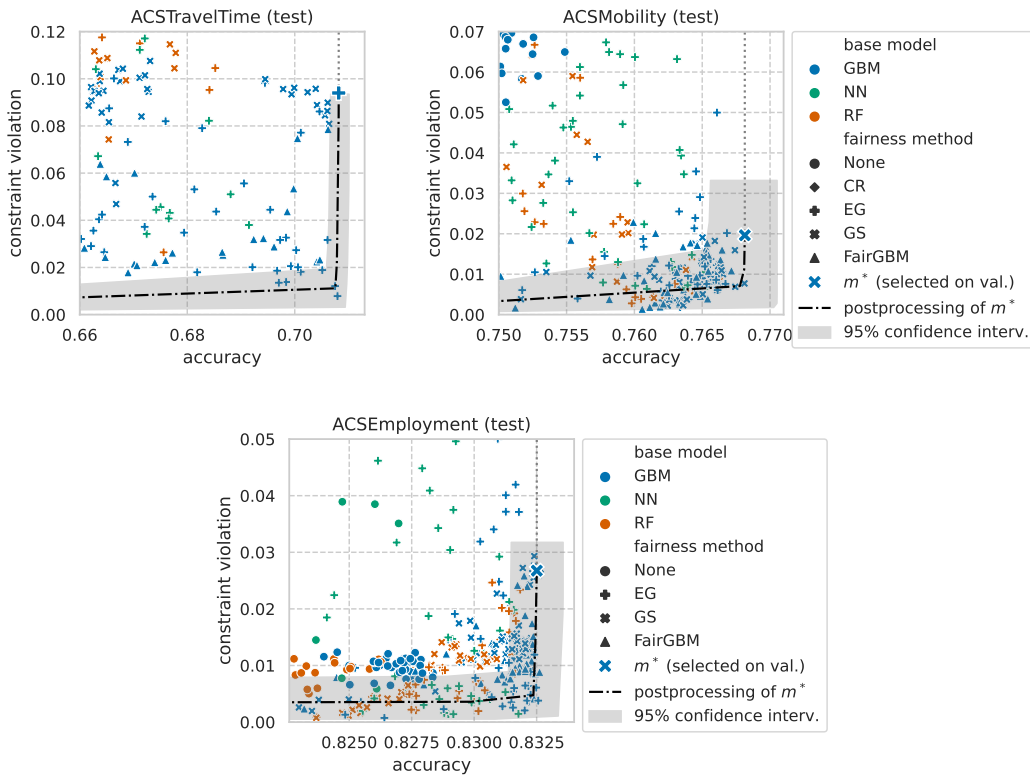


Figure A14: **[Binary protected groups]** Detailed view of the postprocessing Pareto frontier on the ACSTravelTime (left), ACSMobility (right), and ACSEmployment (bottom) datasets, when using only samples of the two largest groups (*White* and *Black*). Note the significantly reduced y axis range (constraint violation) when compared with main experiment results, which use four sensitive groups.

## C Experiment run details

All experiments were ran on as jobs submitted to a centralized cluster, running the open-source HTCondor scheduler. Each job was given the same computing resources: 1 CPU. Compute nodes use AMD EPYC 7662 64-core CPUs. Memory was allocated as required for each algorithm: all jobs were

allocated at least 8GB of RAM; GS and EG jobs were allocated 64GB of RAM as these algorithms will train multiple instances of the underlying base model, increasing memory requirements.

An experiment (a job) accounts for training and evaluating a single model on a given dataset. That is, 1000 experiments were ran on each dataset (50 per algorithm type), totaling 10K experiments (5K for the main experiment using 4 sensitive groups, and 5K for the experiment using 2 sensitive groups). Hyperparameters are randomly sampled at the beginning of each experiment. Detailed hyperparameter search spaces for each algorithm are included in folder `hyperparameters` of the supplementary materials' files.<sup>2</sup>

Complete code base required to replicate experiments is provided as part of the supplementary materials, together with exact evaluation results for each trained model, and code to generate the paper plots.<sup>2</sup>

## D Thresholding group-calibrated predictors

In this section we provide a proof for the following statement: for any classifier with group-calibrated scores (Equations 8–9), the group-specific decision thresholds that minimize the classification loss among each group all take the same value,  $t_a = t_b, \forall a, b \in \mathcal{S}$ , which is fully determined by the loss function,  $t_s = \frac{\ell(1,0)}{\ell(1,0)+\ell(0,1)}, \forall s \in \mathcal{S}$ .

Given a joint distribution over features, labels, and sensitive attributes  $(X, Y, S)$ , a binary classification loss function  $\ell : \{0, 1\}^2 \rightarrow \mathbb{R}^+$ , predictive scores  $R = f(X)$ , and binary predictions  $\hat{Y} = \mathbb{1}\{R \geq t\}, t \in \mathcal{T} \subseteq \mathbb{R}$ . Assume the scores  $R$  are *group-calibrated* [4], i.e.:

$$\mathbb{P}[Y = 1|R = r, S = s] = r, \quad \forall r \in [0, 1], \quad \forall s \in \mathcal{S}, \quad (8)$$

$$\mathbb{P}[Y = 0|R = r, S = s] = 1 - r, \quad \forall r \in [0, 1], \quad \forall s \in \mathcal{S}. \quad (9)$$

We want to minimize the expected loss among samples of group  $s$ ,  $L_s(t) = \mathbb{E}[\ell(\hat{Y}, Y)|S = s]$ :

$$L_s(t) = \ell(1, 0) \cdot \mathbb{P}[\hat{Y} = 1, Y = 0|S = s] + \ell(0, 1) \cdot \mathbb{P}[\hat{Y} = 0, Y = 1|S = s], \quad (10)$$

assuming w.l.o.g. no cost for correct predictions  $\ell(0, 0) = \ell(1, 1) = 0$ .

We have:

$$\mathbb{P}[\hat{Y} = 1, Y = 0|S = s] = \mathbb{P}[\hat{Y} = 1|Y = 0, S = s] \cdot \mathbb{P}[Y = 0|S = s] = h_s^{\text{FP}}(t) \cdot \mathbb{P}[Y = 0|S = s],$$

$$\mathbb{P}[\hat{Y} = 0, Y = 1|S = s] = \mathbb{P}[\hat{Y} = 0|Y = 1, S = s] \cdot \mathbb{P}[Y = 1|S = s] = h_s^{\text{FN}}(t) \cdot \mathbb{P}[Y = 1|S = s],$$

where  $h_s^{\text{FP}}(t)$  and  $h_s^{\text{FN}}(t)$  are, respectively, the False Positive Rate (FPR) and the False Negative Rate (FNR) among samples of group  $s$ , as functions of the chosen group-specific threshold  $t$ . We can trade-off FPR and FNR by varying the threshold, leading to a 2-dimensional curve known as the Receiver Operating Characteristic (ROC) curve.

<sup>2</sup>Supplementary materials available at: <https://github.com/AndreFCruz/error-parity/tree/supp-materials>



Furthermore, given the conditional density function of  $R$  given  $S = s$ ,  $p_{R|s}(r)$ , we have:

$$\begin{aligned}
h_s^{\text{FP}}(t) &= \mathbb{P}[\hat{Y} = 1 | Y = 0, S = s] \\
&= \mathbb{P}[R \geq t | Y = 0, S = s] \\
&= \frac{\mathbb{P}[Y = 0 | R \geq t, S = s] \cdot \mathbb{P}[R \geq t | S = s]}{\mathbb{P}[Y = 0 | S = s]} \\
&= \int_t^1 \frac{(1-r) \cdot p_{R|s}(r)}{\mathbb{P}[Y = 0 | S = s]} dr, &> \text{using calibration (Eq. 9)} \\
\frac{\partial h_s^{\text{FP}}}{\partial t} &= \frac{(t-1) \cdot p_{R|s}(t)}{\mathbb{P}[Y = 0 | S = s]},
\end{aligned}$$

and,

$$\begin{aligned}
h_s^{\text{FN}}(t) &= \mathbb{P}[\hat{Y} = 0 | Y = 1, S = s] \\
&= \mathbb{P}[R < t | Y = 1, S = s] \\
&= \frac{\mathbb{P}[Y = 1 | R < t, S = s] \cdot \mathbb{P}[R < t | S = s]}{\mathbb{P}[Y = 1 | S = s]} \\
&= \int_0^t \frac{r \cdot p_{R|s}(r)}{\mathbb{P}[Y = 1 | S = s]} dr, &> \text{using calibration (Eq. 8)} \\
\frac{\partial h_s^{\text{FN}}}{\partial t} &= \frac{t \cdot p_{R|s}(t)}{\mathbb{P}[Y = 1 | S = s]}.
\end{aligned}$$

The threshold  $t_s$  that minimizes the group-specific loss  $L_s(t)$  is a solution to  $\frac{\partial L_s}{\partial t} = 0$ , where:

$$\begin{aligned}
L_s(t) &= \ell(1, 0) \cdot h_s^{\text{FP}}(t) \cdot \mathbb{P}[Y = 0 | S = s] + \ell(0, 1) \cdot h_s^{\text{FN}}(t) \cdot \mathbb{P}[Y = 1 | S = s], \\
\frac{\partial L_s}{\partial t} &= \ell(1, 0) \cdot (t-1) \cdot p_{R|s}(t) + \ell(0, 1) \cdot t \cdot p_{R|s}(t).
\end{aligned}$$

Hence, for a group-calibrated predictor (fulfilling Equations 8–9), for any group  $s \in \mathcal{S}$ , the optimal group-specific decision threshold  $t_s$  does not depend on any group quantities, and is given by:

$$t_s = \frac{\ell(1, 0)}{\ell(1, 0) + \ell(0, 1)}.$$